Dissolution of SiO_2 Inclusions in CaO-SiO_2-Based Slags *In Situ* Observed Using High-Temperature Confocal Scanning Laser Microscopy

YING REN, PEI ZHU, CHANGYU REN, NAN LIU, and LIFENG ZHANG

In the current study, the dissolution mechanism of SiO_2 inclusion particles in CaO-SiO_2-based refining slags at 1793 K-1853 K was investigated using high-temperature confocal scanning laser microscopy. The rate-limiting step of the SiO_2 inclusion dissolution in CaO-SiO_2-based refining slags was the diffusion of SiO_2 in CaO-SiO_2-based slags when the boundary layer was formed. The main influence factor of the dissolution rate of SiO_2 inclusions changed from the concentration gradient and the interface area to the interface area during the particle dissolution process. With the increase of the CaO/SiO_2 ratio of slag from 0.5 to 1.25, the dissolution time of the inclusion obviously decreased, indicating that a higher CaO/SiO_2 ratio of slag was beneficial to the removal of inclusions by the slag absorption. The dissolution rate of inclusions increased first and then decreased with higher Al_2O_3 content. The optimal Al_2O_3 content of CaO-SiO_2-Al_2O_3-3 pct MgO slag was 5 pct to promote the inclusion removal. The higher experimental temperature promoted the dissolution of SiO_2 inclusions in slags. A linear relationship between the dissolution rate of SiO_2 particles (v) and a ratio of concentration difference and slag viscosity ($\Delta C/\eta$) was fitted as $v = 800.29 \times \Delta C/\eta$. The dissolution rate of SiO_2 inclusions in CaO-SiO_2-Al_2O_3-3 pct MgO slags commonly used for the Si-Mn-killed steels was predicted.

https://doi.org/10.1007/s11663-021-02401-5

I. INTRODUCTION

NON-METALLIC inclusions are a key issue in the production of clean steels. Inclusion characters, including composition, size, number, and distribution, were related to the steel performance. During the secondary refining process, the slag composition and refining time were adjusted to remove inclusions and improve the steel cleanliness. Thus, it was necessary to investigate the inclusion dissolution behaviors in the refining slag. The avoid formation of undeformed Al_2O_3 inclusions with the high melting temperature after the aluminum deoxidation, silicon deoxidation was applied. However, silicate inclusions were generated after silicon deoxidation, which was detrimental to the steel quality. Thus, it was important to investigate the effect of the refining slag composition on the dissolution of inclusions.

Dissolution kinetics of inclusion particles in the refining slag were traditionally investigated through the dip test. Dipped materials included refractory rods,[1] inclusions,[2,3] and crucibles.[4,5] The change in the diameter of dipped materials was measured to reveal dissolution kinetics of inclusions in slag. The dissolution of inclusions in slag under various ladle stirring conditions was simulated by adjusting the rotation rate of the refractory. The dip test was also appropriate for investigations of the inclusion dissolution in non-transparent refining slags containing FeO and MnO. Thereafter, there was a huge difference between the inclusion size on the micrometer scale and the dipped rod size on the millimeter scale, which had an influence on the accuracy of experimental results.

High-temperature confocal scanning laser microscopy (CSLM) was widely used in steelmaking studies to observe the evolution of the sample surface during the heating process in situ.[6–11] The dissolution behavior of inclusions in the micrometer scale can be observed in situ and recorded using CSLM. Sridhar *et al.*[12] first observed the dissolution process of inclusions in the

YING REN is with the School of Metallurgical and Ecological Engineering, University of Science and Technology Beijing (USTB), Beijing, 100083 P.R. China and also with the Key Laboratory for Ecological Metallurgy of Multimetallic Ores (Ministry of Education), Northeastern University, Shenyang 110819, P.R. China. PEI ZHU, CHANGYU REN, and NAN LIU are with the School of Metallurgical and Ecological Engineering, University of Science and Technology Beijing (USTB). LIFENG ZHANG is with the State Key Laboratory of Metastable Materials Science and Technology, Yanshan University, Qinhuangdao City, Hebei Province, 066004, P.R. China. Contact e-mail: zhanglifeng@ysu.edu.cn

Manuscript submitted August 19, 2021; accepted November 19, 2021.
Article published online January 21, 2022.

molten slag in situ. Many researchers investigated dissolution kinetics of inclusions in the molten slag using the CSLM,[13–28] as shown in Figure 1. Previous studies mainly focused on the dissolution mechanism of inclusions in the CaO-Al_2O_3-SiO_2 refining slag containing 30 to 70 pct SiO_2 since the slower dissolution rate of inclusions in the slag with the high viscosity and low melting temperature was easier to observe in situ using CSLM. However, CaO-Al_2O_3-SiO_2 refining slag was little used for slag refining of Si-Mn-killed steels. CaO-SiO_2-based refining slag with little Al_2O_3 was widely used to avoid the formation of Al_2O_3 inclusions in Si-Mn-killed steels.[29,30] Feichtinger *et al.*[19] reported that the dissolution rate of SiO_2 in Al_2O_3-SiO_2-CaO slags with 10 to 26 pct Al_2O_3 was related to the slag viscosity. Tian *et al.*[23] investigated the effect of Al_2O_3 and MgO contents on the dissolution rate of SiO_2 in Al_2O_3-SiO_2-CaO-MgO slags with 10 to 26 pct Al_2O_3. However, more investigations were necessary to reveal the dissolution schematic of SiO_2 inclusions in CaO-SiO_2-based refining slags commonly used for Si-Mn-deoxidized steels, as the gray region illustrated in Figure 1.

In the current study, the dissolution mechanism of SiO_2 inclusions in CaO-SiO_2-based refining slags at 1793-1853 K was studied. Effects of the slag basicity and Al_2O_3 content on the dissolution rate of SiO_2 inclusions were investigated through in situ observation using CSLM.

II. EXPERIMENTAL APPROACH

Dissolution behaviors of SiO_2 inclusions in CaO-SiO_2-based refining slags were observed in situ using CSLM (VL2000DX-SVF18SP). The maximum heating and cooling rates were 300 K/s and 100 K/s, respectively. The temperature was calibrated using the melting test using copper with 99.9 wt pct purity. Compositions and parameters of the refining slag commonly used for Si-Mn-killed steels are listed in Table I. The melting temperature, viscosity (η), and SiO_2 solubility in slag were calculated using Factsage 7.0.[31] The slag density (ρ) was calculated using Mills model.[32] The temperature (T), mass ratio of CaO/SiO_2 in slag (C/S), mass ratio of CaO/(SiO_2 + Al_2O_3) (C/(S + A)), viscosity of slag (η), concentration differences of SiO_2 (ΔC), initial radius of SiO_2 particles (R_0), and total dissolution time (t_{total}) were also listed. The refining slag was mixed using powders of Al_2O_3 (> 99 wt pct, Sinopharm), SiO_2 (> 99 wt pct, Sinopharm), and CaO (> 98 wt pct, Xilong Scientific).

Mixed powders were pre-melted at 1873 K at the argon atmosphere to homogenize the slag composition. Slag samples were quenched and broken and then ground in an agate crucible for 15 to 30 minutes. The composition of the slag was analyzed using x-ray fluorescence spectrometer. Slag powders were pressed into a cylinder with 5 mm diameter and 4 mm height and then melted and quenched in a platinum crucible to obtain transparent slags. The inclusion particle was placed on the surface of the slag sample, as shown in Figure 2. To ensure the stable composition of slag, the mass of selected inclusion particles was < 0.2 pct of the slag quality. The temperature curve of CSLM observation during heating and cooling processes is illustrated in Figure 3. The temperature was heated to 50 K under the target temperature at a heating rate of 1000 K/min. Then, the heating rate was lowered to 300 K/min to avoid the over-shot of the temperature and improve the accuracy of the start time. The time was counted after the temperature reached the target observation temperature. Figure 4 shows images of the typical SiO_2 inclusion dissolution process in the CaO-SiO_2-based slag. After the temperature reached the target observation temperature of 1823 K, there was an obvious border line between the ellipsoidal inclusion particle and bulk slag. The average initial R_0 of the inclusion particle was roughly 200 μm. During the dissolution process of inclusions, the size of the inclusion gradually decreased and the shape of the inclusion trended to be spherical. More than 30 s after the temperature reached 1823 K, the inclusion particle was totally dissolved in the slag.

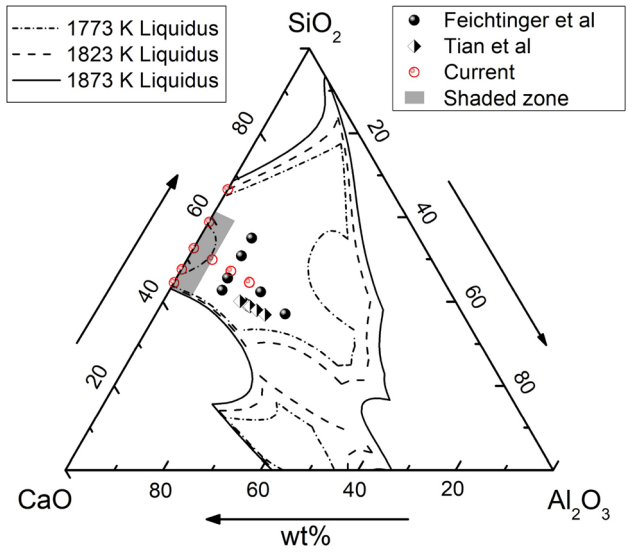

Fig. 1—Summarized investigations[19,23] on the dissolution of SiO_2 in refining slags.

III. DISSOLUTION OBSERVATION OF SIO_2 INCLUSIONS IN CAO-AL_2O_3-SIO_2 SLAGS

A. *Dissolution Mechanism of SiO_2 Inclusions in Slag*

There were two classic models for the dissolution mechanism of inclusions in slags, including the unreacted core model[33] and the diffusion equation.[34–36] The rate-limiting step of the unreacted core model was the reaction at the interface and the diffusion at the boundary layer. When the interfacial reaction was the limiting step of the inclusion dissolution, the dissolution period of the inclusion showed a linear relationship with its radius, as expressed in Eqs. [1] and [2].[33] When the boundary layer diffusion was the limiting step, the dissolution period of inclusions was linearly related to

Table I. Experimental Parameters for the SiO_2 Dissolution in Slag

Slag	SiO_2	CaO	MgO	Al_2O_3	C/S	C/(S + A)	T (K)	η (Pa·s)	ρ (kg/m^3)	ΔC (kg/m^3)	R_0 (μm)	t_{total} (s)
1	43.1	53.9	3.0	0	1.25	—	1793	0.172	2468	485	209	27
							1823	0.147	2460	504	203	11
							1853	0.126	2453	526	206	9
2	46.2	50.8	3.0	0	1.10	—	1793	0.213	2451	416	214	47
							1823	0.181	2444	436	203	16
							1853	0.155	2437	458	203	14
3	48.5	48.5	3.0	0	1.00	—	1793	0.255	2439	365	206	49
							1823	0.216	2432	385	198	24
							1853	0.184	2425	407	202	19
4	51.0	46.0	3.0	0	0.90	—	1793	0.320	2426	310	213	57
							1823	0.271	2419	331	203	33
							1853	0.230	2412	353	199	26
5	53.9	43.1	3.0	0	0.80	—	1793	0.426	2411	249	202	67
							1823	0.359	2403	269	202	48
							1853	0.304	2397	291	208	47
6	57.0	40.0	3.0	0	0.70	—	1793	0.614	2394	182	201	169
							1823	0.514	2387	203	196	85
							1853	0.433	2380	226	201	72
7	64.7	32.3	3.0	0	0.50	—	1793	1.804	2355	26	205	3774
							1823	1.486	2348	48	198	1325
							1853	1.233	2341	71	202	803
8	48.4	43.6	3.0	5.0	—	0.82	1793	0.341	2485	402	203	36
							1823	0.287	2477	423	212	29
							1853	0.243	2470	445	207	24
9	45.8	41.2	3.0	10.0	—	0.74	1793	0.404	2543	489	206	39
							1823	0.337	2536	510	204	31
							1853	0.284	2528	533	188	25
10	43.2	38.8	3.0	15.0	—	0.67	1793	0.494	2602	573	200	38
							1823	0.409	2594	593	201	33
							1853	0.342	2586	617	194	30

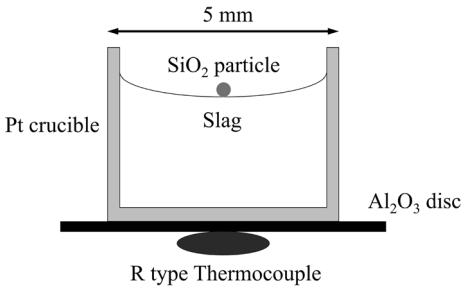

Fig. 2—Placement schematic of inclusion and slag before heating.

the square of inclusion radius in Eqs. [3] and [4].[33] Since the size of inclusions had an important influence on the dissolution rate, the volume of inclusions was used to characterize the dissolution rate in the current study.

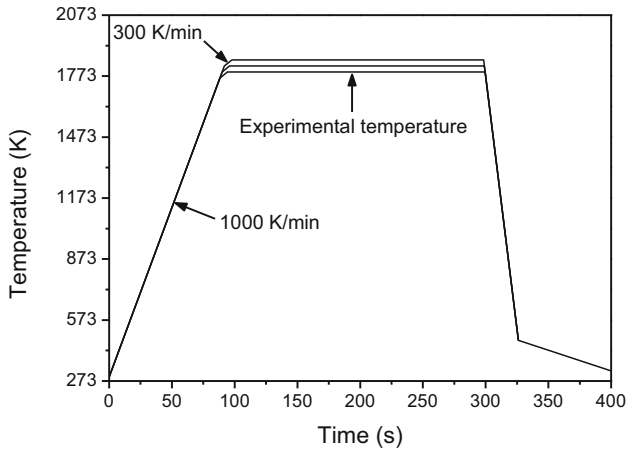

Fig. 3—Temperature curve of the CSLM observation during heating and cooling processes.

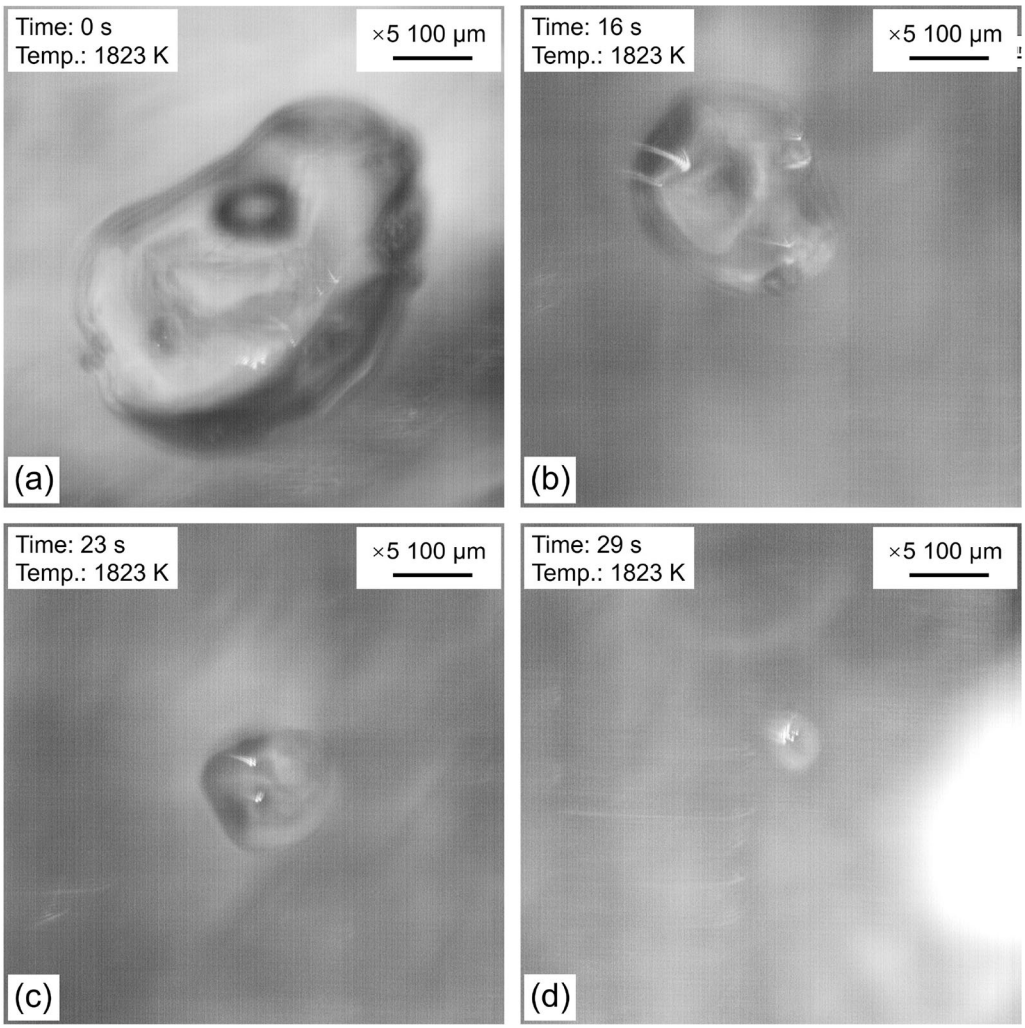

Fig. 4—Images of the typical dissolution process of the SiO_2 inclusion in the CaO-SiO_2-based slag: (*a*) 0 s, (*b*) 16 s, (*c*) 23 s, and (*d*) 29 s.

$$\tau = \frac{\rho_p R_0}{bK\Delta C} \quad [1]$$

$$\frac{V}{V_0} = \left(1 - \frac{t}{\tau}\right)^3 \quad [2]$$

$$\tau = \frac{\rho_p R_0^2}{2b\Delta CD} \quad [3]$$

$$\frac{V}{V_0} = \left(1 - \frac{t}{\tau}\right)^{1.5} \quad [4]$$

where τ is the dissolution period for the particle, s; D is the diffusion coefficient of the solute in the boundary layer,$m^2 \cdot s^{-1}$; ρ_p is the particle density, kg/m^3; R_0 is the initial radius of the particle, μm; K is the first order rate constant of the reaction, s^{-1}; ΔC is the supersaturation of inclusions in slag, wt pct; b is the stoichiometric number.

Liu[16] and Feichtinger[19] *et al.* described the dissolution mechanism of inclusions by the diffusion equation. At the beginning of the inclusion dissolution, the concentration boundary layer around the inclusion was hardly formed. The larger concentration gradient resulted the dissolution rate of the inclusion faster than calculated results using the unreacted core model. During the dissolution process, the concentration gradient showed a decreasing trend, and the dissolution rate of inclusions tended to be stable, as given in Eqs. [5] through [7].[34–36] In addition, the Lattice Boltzmann model (LBM)[37] based on the diffusion equation was proposed to better describe dissolution kinetics of inclusions, which was seldom applied because of its calculation complexity.

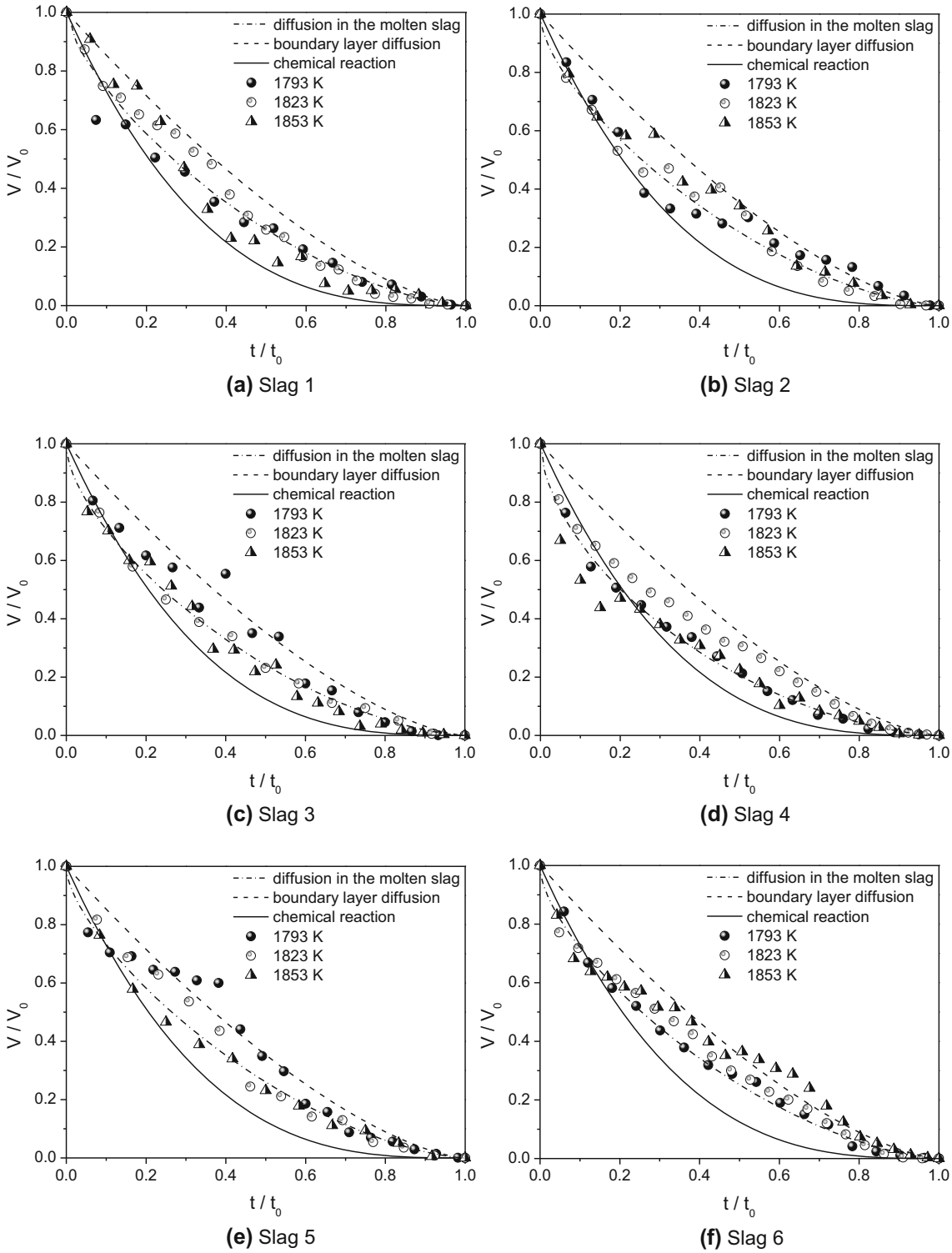

Fig. 5—Comparison between the measured curve of the inclusion dissolution in slag and the predicted curve using the three mentioned models: (*a*) through (*g*) Slag 1 to 7.

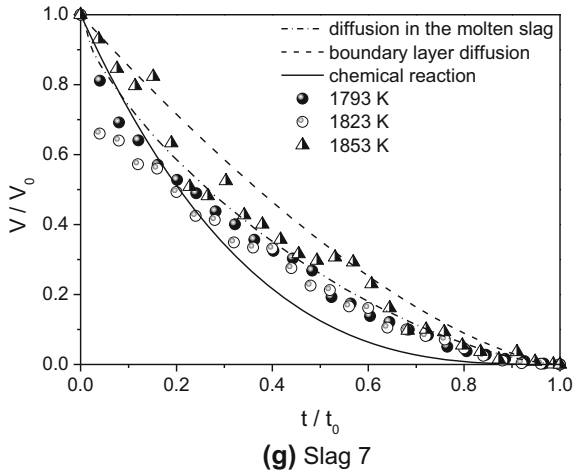

Fig. 5—continued.

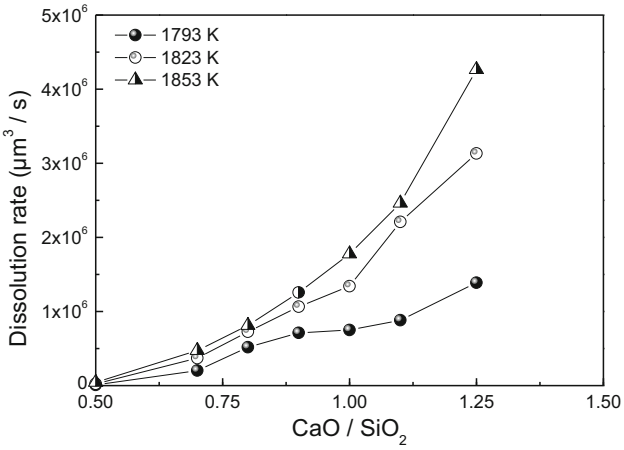

Fig. 7—Curves of SiO_2 inclusions dissolved in the CaO-SiO_2-based refining slag with various C/S ratios at various temperatures.

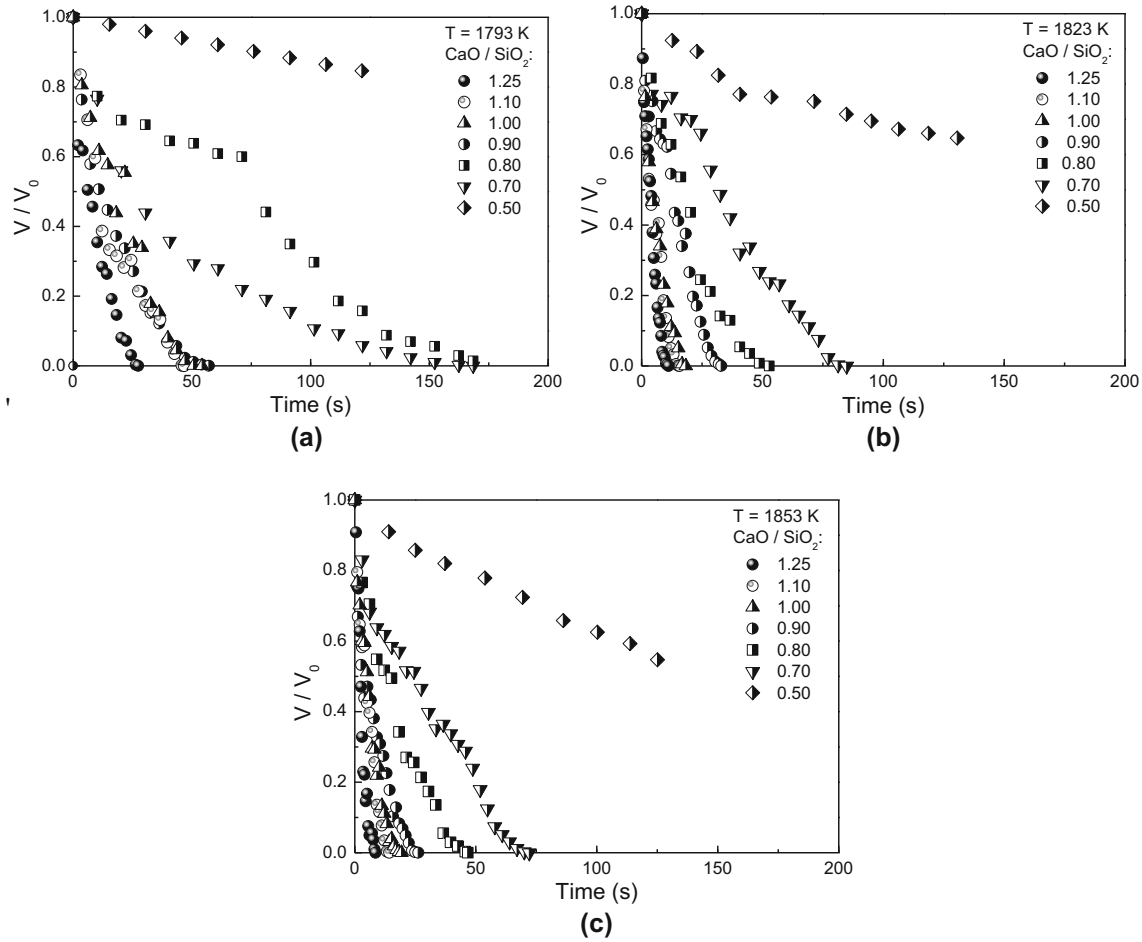

Fig. 6—Curves of SiO_2 inclusions dissolved in the CaO-SiO_2-based refining slag with various C/S ratios at various temperatures: (*a*) 1793 K, (*b*) 1823 K, (*c*) 1853 K.

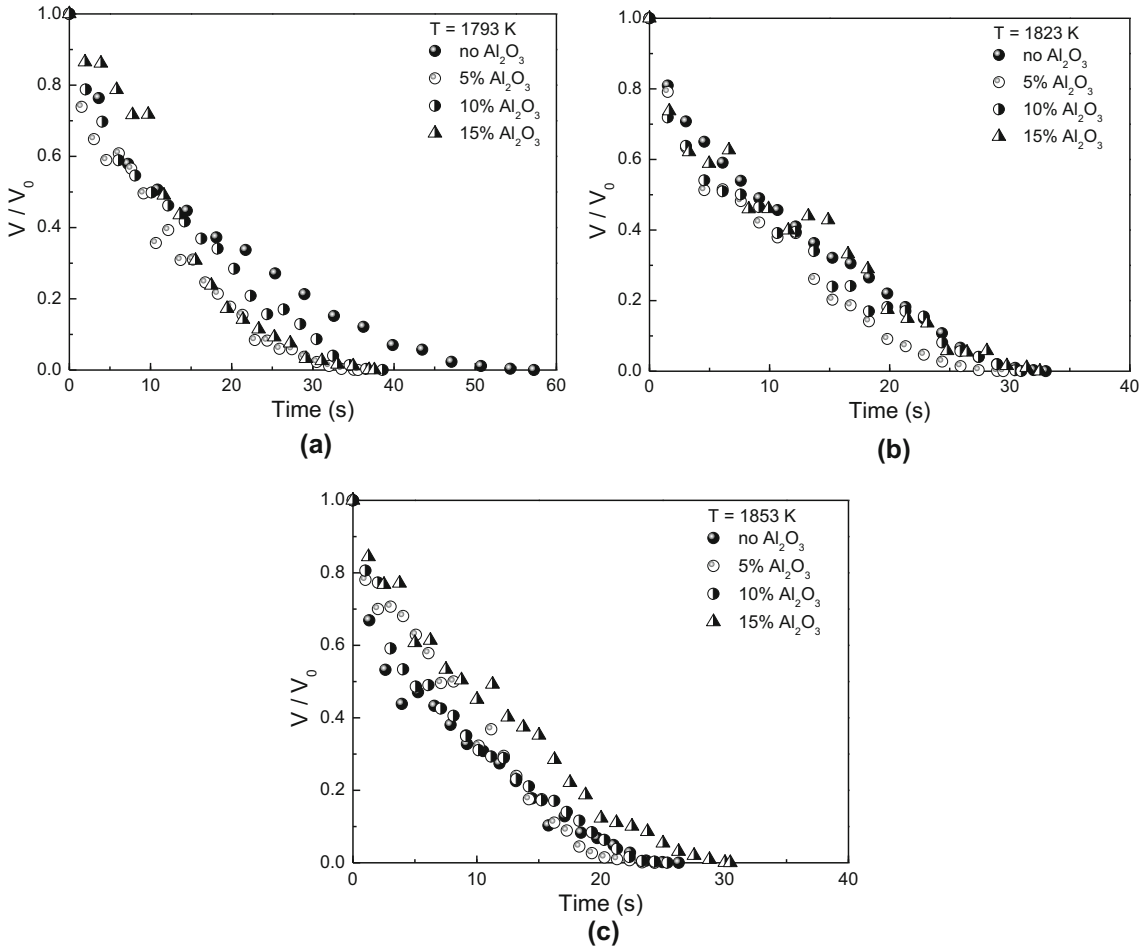

Fig. 8—Curves of SiO_2 inclusions dissolved in the CaO-SiO_2-based refining slag with various Al_2O_3 contents: (*a*) 1793K, (*b*) 1823 K, (*c*) 1853 K.

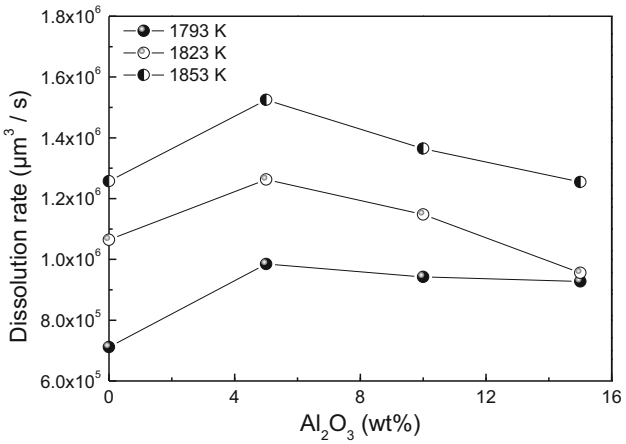

Fig. 9—Curves of SiO_2 inclusions dissolved in the CaO-SiO_2-based refining slag with various Al_2O_3 contents at 1793 K, 1823 K, and 1853 K.

$$\frac{\mathrm{d}R}{\mathrm{d}t} = -\frac{k_0 \cdot D}{R} - k_0 \cdot \sqrt{\frac{D}{\pi \cdot t}} \qquad [5]$$

$$k_0 = \frac{c_\mathrm{s} - c_\mathrm{b}}{c_\mathrm{p} - c_\mathrm{s}} \qquad [6]$$

$$c = \rho \cdot x \qquad [7]$$

where c_b, c_s, and c_p are the mass concentration of solute in slag, saturated slag and inclusion particles, kg m^{-3}; k_0 is the dimensionless saturation;ρ was the slag density of, kg m^{-3};x is the mass percentage of solute in the slag, wt pct.

Based on the above three rate-limiting steps, the dissolution mechanism of SiO_2 inclusions was investigated through the comparison between the measured curve of the inclusion dissolution in slag and the predicted curve using the three models mentioned in Figure 5. Various shapes represented experimental points at different temperatures. In the early stage of the SiO_2 dissolution in slag, the dissolution curve was consistent with both the chemical reaction model and diffusion in the molten slag model because the boundary layer around the SiO_2 particle was not formed. Then, the dissolution curve of the SiO_2 inclusion in slag was in line with the diffusion in the molten slag model,

indicating that the main rate-limiting step was the diffusion of SiO_2 in CaO-SiO_2-based slags. At the start of the inclusion dissolution, the large concentration gradient between the inclusion and the bulk slag led to a higher dissolution rate of SiO_2 inclusions than the prediction of the unreacted core model. During the dissolution of the inclusion, the concentration gradient between the inclusion and the slag became smaller, lowering the decrease of the dissolution rate of SiO_2 particles. Meanwhile, the interface area of slag and particle decreased, which lowered the dissolution rate of inclusions in slag. Thus, the main influence factor of the dissolution rate of SiO_2 inclusions changed from the concentration gradient and the interface area to the interface area during the particle dissolution process.

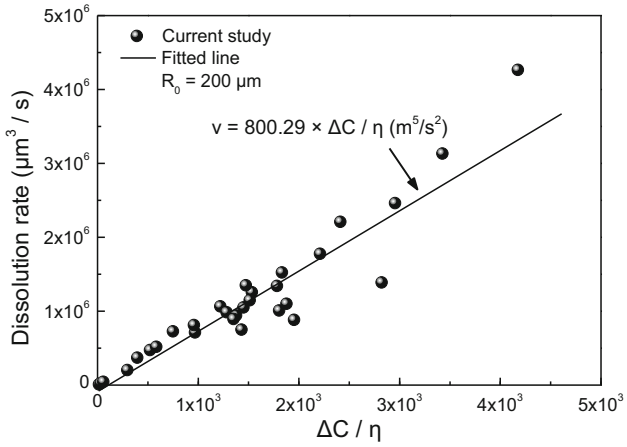

Fig. 11—Relationship between the dissolution rate of SiO_2 and $\Delta C/\eta$.

B. *Effect of C/S Ratio and Al_2O_3 Contents on the Dissolution Rate*

The dissolution curve of SiO_2 particles in CaO-SiO_2-based slags with various C/S ratios is shown in Figure 6. With the increase of the C/S ratio from 0.5 to 1.25, the dissolution time of the inclusion obviously decreased, indicating that the higher C/S ratio of slag was beneficial to the removal of inclusions from the molten steel. The dissolution volume fraction of SiO_2 inclusions was < 50 pct after 130 s of the inclusion dissolution in the slag with a ratio of 0.50, while the dissolution time of inclusions was < 25 s of the inclusion dissolution for the slag with a ratio of 1.25. The dissolution rates (v) of SiO_2 particles in CaO-SiO_2-based slags with various C/S ratios at various temperatures are shown in Figure 7. The dissolution rate of inclusions was obviously enhanced by the higher C/S ratio and the temperature. It was noted that the dissolution time was significantly related to the temperature. For the slag with the C/S ratio of 1.25, the dissolution rate rose from 1.38×10^{-6} $\mu m^3/s$ to 4.26×10^{-6} $\mu m^3/s$ with the temperature from 1793 K to 1853 K. It was necessary to increase the refining temperature to promote the inclusion removal by the slag absorption.

The dissolution curve of SiO_2 particles in CaO-SiO_2-based slags with various Al_2O_3 contents is shown in Figure 8. With the increase of the Al_2O_3 content from 0 to 15 pct, the dissolution time of inclusions first decreased and then increased, indicating that there was an optimal value of the Al_2O_3 content in the CaO-SiO_2-based slag to improve the removal of inclusions. The dissolution time of SiO_2 inclusions in the slag with the C/S ratio of 0.9 was in the range of 25 to 60 seconds. The higher temperature was beneficial to the removal of inclusions. The dissolution rates of SiO_2 inclusions in CaO-SiO_2-based refining slags with various Al_2O_3 contents at various temperatures are shown in Figure 9. The dissolution rate of inclusions increased first and then decreased with the higher Al_2O_3 content, reaching a maximum value for the slag with 5 pct Al_2O_3. The fluctuation of the dissolution rate of

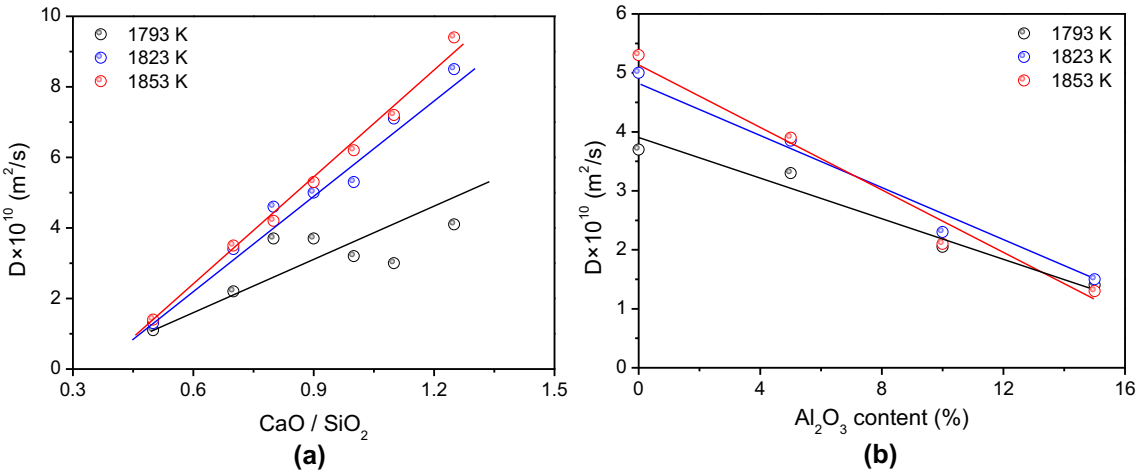

Fig. 10—Diffusion coefficients of the particle predicted by the diffusion in slag control model: (*a*) D vs CaO/SiO_2, (*b*) D vs Al_2O_3 content.

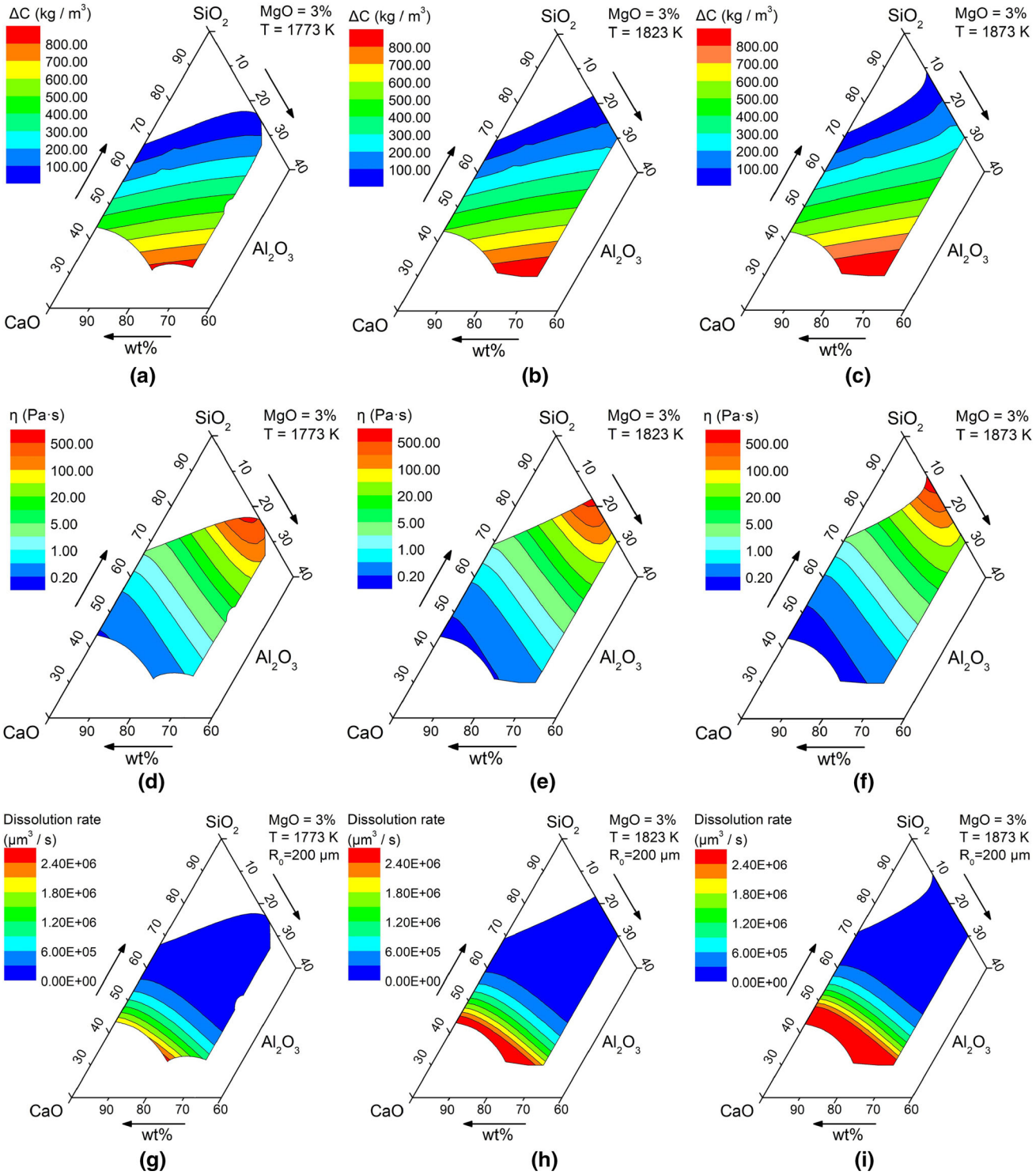

Fig. 12—Prediction of the ΔC, η, and v of the SiO_2 particle in the Al_2O_3-SiO_2-CaO-3 pct MgO slag at 1773 K, 1823 K, and 1873 K: (*a*) to (*c*) ΔC, (*d*) to (*f*) η, (*g*) to (*i*) v.

inclusions was mainly influenced by the slag viscosity and the concentration difference of SiO_2. It was noted that increasing the refining temperature was the most effective way to improve the inclusion removal by the slag absorption.

C. *Prediction of SiO_2 Dissolution Rate*

To better understand the dissolution behavior of SiO_2 inclusions in CaO-SiO_2-based slags, diffusion coefficients for various slags were calculated using the diffusion in slag control model. The dimensionless

saturation was calculated using Eqs. [6] and [7]. Then, diffusion coefficients can be calculated using Eq. [5]. Figure 10 shows diffusion coefficients of the particle predicted by the diffusion in slag control model. Diffusion coefficients increased with the increase of the C/S ratio of slag from 0.5 to 1.25, while it decreased with a higher Al_2O_3 content from 0 to 15 pct. The higher the temperature is, the larger value of diffusion coefficients.

It was reported that the dissolution rate of inclusions was mainly determined by the slag viscosity and concentration differences,[38] which was significantly related to the slag composition and the inclusion. The relationship between the dissolution rate of SiO_2 and $\Delta C/\eta$ is shown in Figure 11. The ΔC and η of Slags 1 to 10 at various temperatures were calculated using FactSage thermodynamic software, which are listed in Table I. The dissolution rate of SiO_2 linearly increased with a higher $\Delta C/\eta$. A linear relationship between the dissolution rate of SiO_2 and $\Delta C/\eta$ was fitted as Eq. [8], which can be used for the prediction of the dissolution rate of SiO_2 inclusions in CaO-SiO_2-based slags. To better understand the SiO_2 absorption ability of CaO-SiO_2-based slag, many calculations using FactSage were conducted for the commonly used CaO-SiO_2-Al_2O_3-3 pct MgO slags, as shown in Figure 12. The ΔC and η of liquid slags with < 30 pct of Al_2O_3 content at 1773 K, 1823 K, and 1873K were calculated using FactSage, considering > 300 compositions of liquid CaO-SiO_2-Al_2O_3-3 pct MgO slags. The concentration difference increased with a lower SiO_2 content of slag. The slag viscosity was effectively increased by the addition of CaO in slag. The ΔC and η of slags increased at a higher temperature. The dissolution rate of SiO_2 inclusions in CaO-SiO_2-Al_2O_3-3 pct MgO slags was predicted by substituting the calculated ΔC and η to Eq. [8].

$$V = 800.29 \times \Delta C/\eta. \quad [8]$$

IV. CONCLUSIONS

In the current study, the dissolution mechanism of SiO_2 inclusions in CaO-SiO_2-based refining slags at 1793 K to 1853 K was studied to optimize the slag composition of the Si-Mn-killed steels. Effects of the slag basicity, Al_2O_3 content, and temperature on the dissolution rate of SiO_2 inclusions were investigated through in situ observation using CSLM.

1. The rate-limiting step of the SiO_2 inclusion dissolution in CaO-SiO_2-based refining slags was the diffusion of SiO_2 in CaO-SiO_2-based slags when the boundary layer was formed. The main influence factor of the dissolution rate of SiO_2 inclusions changed from the concentration gradient and the interface area to the interface area during the particle dissolution process.
2. With the increase of the C/S ratio from 0.5 to 1.25, the dissolution time of the inclusion obviously decreased. The dissolution rate of inclusions increased first and then decreased with higher Al_2O_3 content, reaching a maximum value for the slag with 5 pct Al_2O_3. The higher refining temperature promoted the inclusion removal by the slag absorption.
3. A linear relationship between the dissolution rate of SiO_2 and $\Delta C/\eta$ was fitted as $v = 800.29 \times \Delta C/\eta$. The dissolution rate of SiO_2 inclusions in CaO-SiO_2-Al_2O_3-3 pct MgO slags with various compositions was predicted.

ACKNOWLEDGMENTS

The authors are grateful for support from the National Nature Science Foundation of China (Grant Nos. U1860206, 51725402), the S&T Program of Hebei (Grant Nos. 20311004D, 20311005D, 20311006D, 20591001D), the High Steel Center (HSC) at Yanshan University, Beijing International Center of Advanced and Intelligent Manufacturing of High Quality Steel Materials (ICSM) and the High Quality Steel Consortium (HQSC) at University of Science and Technology Beijing (USTB), China, and Key Laboratory for Ecological Metallurgy of Multimetallic Ores (Ministry of Education) Fund.

CONFLICT OF INTEREST On behalf of all authors, the corresponding author states that there is no conflict of interest.

REFERENCES

1. B. Yu, X. Lv, S. Xiang, and X. Jian: *Metall. Mater. Trans. B*, 2016, vol. 47B, pp. 2063–71.
2. W.D. Cho and P. Fan: *ISIJ Int.*, 2004, vol. 44, pp. 229–34.
3. L. Zhang, M. Chen, M. Huang, N. Wang, and C. Wang: *Metall. Mater. Trans. B*, 2021, vol. 52, pp. 2703–14.
4. K. Goto, B.B. Argent, and W.E. Lee: *J Am Ceram Soc*, 2005, vol. 80, pp. 461–71.
5. T. Miki and A. Kawakami: *ISIJ Int.*, 2020, vol. 60, pp. 1434–37.
6. L. Gao, M. Ma, H. Hu, and Z. Yan: *Int. J. Miner. Met. Mater.*, 2019, vol. 26, pp. 483–92.
7. S. Li, G. Cheng, Z. Miao, L. Chen, and X. Jiang: *Int. J. Miner. Met. Mater.*, 2019, vol. 26, pp. 291–300.
8. J. Guo, X. Chen, S. Han, Y. Yan, and H. Guo: *Int J Min Met Mater*, 2020, vol. 27, pp. 328–39.
9. X. Zhao, Z. Yang, and F. Zhang: *Int. J. Miner. Met. Mater.*, 2020, vol. 27, pp. 620–29.
10. D. Fu, G. Wen, X. Zhu, J. Guo, and P. Tang: *J. Iron Steel. Res. Int.*, 2021, vol. 28, pp. 1133–40.
11. J.H. Kim, S.G. Kim, and A. Inoue: *Acta Mater.*, 2001, vol. 49, pp. 615–22.
12. S. Sridhar and A.W. Cramb: *Metall. Mater. Trans. B*, 2000, vol. 31, pp. 406–10.
13. M. Valdez, K. Prapakorn, A.W. Cramb, and S. Sridhar: *Ironmak Steelmak*, 2002, vol. 29, pp. 47–52.
14. B.J. Monaghan and L. Chen: *J. Non-Cryst. Solids*, 2004, vol. 347, pp. 254–61.
15. B.J. Monaghan and L. Chen: *Steel. Res. Int.*, 2005, vol. 76, pp. 348–54.
16. J. Liu, F. Verhaeghe, M. Guo, B. Blanpain, and P. Wollants: *J. Am. Ceram. Soc.*, 2007, vol. 90, pp. 3818–24.
17. J. Liu, M. Guo, P.T. Jones, F. Verhaeghe, B. Blanpain, and P. Wollants: *J. Eur. Ceram. Soc.*, 2007, vol. 27, pp. 1961–72.
18. J. Liu, L. Zhu, M. Guo, F. Verhaeghe, B. Blanpain, and P. Wollants: *Metall. Res. Technol.*, 2008, vol. 105, pp. 255–62.

19. S. Feichtinger, S.K. Michelic, Y.B. Kang, and C. Bernhard: *J. Am .Ceram. Soc*., 2014, vol. 97, pp. 316–25.
20. P. Yan, B.A. Webler, P.C. Pistorius, and R.J. Fruehan: *Metall. Mater. Trans. B*, 2015, vol. 46, pp. 2414–18.
21. K. Miao, A. Haas, M. Sharma, W. Mu, and N. Dogan: *Metall. Mater. Trans. B*, 2018, vol. 49B, pp. 1612–23.
22. M. Sharma, W. Mu and N. Dogan: Alstech, 2018, pp. 2601–08.
23. T. Tian, Y. Zhang, H. Zhang, K. Zhang, J. Li, and H. Wang: *Int. J. Appl. Ceram. Technol*., 2019, vol. 16, pp. 1–10.
24. Y. Park, Y. Cho, W. Cha, and Y. Kang: *J. Am. Ceram. Soc*., 2020, vol. 103, pp. 2210–24.
25. M. Sharma and N. Dogan: *Metall. Mater. Trans. B*, 2020, vol. 51B, pp. 570–80.
26. Y. Lee, J.K. Yang, D.J. Min, and J.H. Park: *Ceram. Int*., 2019, vol. 45, p. 20251.
27. S. Michelic, J. Goriupp, S. Feichtinger, Y. Kang, C. Bernhard, and J. Schenk: *Steel Res. Int*., 2016, vol. 87, pp. 57–67.
28. A.B. Fox, M. Valdez, and J. Gisby: *ISIJ Int*., 2004, vol. 44, pp. 836–45.
29. Y. Ren, L. Zhang, W. Fang, S. Shao, J. Yang, and W. Mao: *Metall. Mater. Trans. B*, 2016, vol. 47B, pp. 1024–34.
30. T. Yuan, L. Zhang, Y. Ren, Q. Zhao, and C. Liu: *Steel Res. Int*., 2020, vol. 92, p. 2000506.
31. C.W. Bale, P. Chartrand, S.A. Degterov, G. Eriksson, K. Hack, R.B. Mahfoud, J. Melancon, A.D. Pelton, and S. Petersen: *Calphad*, 2002, vol. 26, pp. 189–228.
32. K.C. Mills and B.J. Keene: *Int. Mater. Rev*., 1987, vol. 32, pp. 1–120.
33. O. Levenspiel: *Chemical Reaction Engineering*, Wiley, New York, 1999, pp. 566–88.
34. M.J. Whelan: *Met. Sci. J*., 1969, vol. 3, pp. 95–97.
35. H.B. Aaron, D. Fainstein, and G.R. Kotler: *J Appl Phys*, 1970, vol. 41, pp. 4404–10.
36. LC. Brown: *J Appl Phys*, 1976, vol. 47, pp. 449–58.
37. F. Verhaeghe, S. Arnout, B. Blanpain and P. Wollants: *Phys Rev E*, 2005, vol. 72, pp. 036308.
38. M. Valdez, G.S. Shannon, and S. Sridhar: *ISIJ Int*, 2006, vol. 46, pp. 450–57.